

## Direct co-deposition of mono-sized nanoparticles during sputtering

Mikhail N. Polyakov, Rachel L. Schoeppner, Laszlo Pethö, Thomas E.J. Edwards\*,  
Keith Thomas, Bence Könnyű, Xavier Maeder, Johann Michler

*Empa - Swiss Federal Laboratories for Materials Science and Technology, Feuerwerkerstrasse 39, 3602 Thun, Switzerland*



### ARTICLE INFO

#### Article history:

Received 4 March 2020

Revised 13 May 2020

Accepted 13 May 2020

Available online 5 June 2020

#### Keywords:

Nanocomposites

Nanoparticles

Synthesis

Thermal stability

Sputtering

### ABSTRACT

Nanoparticle-reinforced thin films synthesis is often limited by precipitation thermodynamics and kinetics to certain material combinations and nanoparticle size distributions. We demonstrate a new method that allows direct co-deposition of mono-sized nanoparticles with various matrix materials, independent particle size and composition control, yielding flexible material selection, and nanoparticle density spatial variations laterally and depth-wise. Tungsten nanoparticles were co-deposited into magnetron-sputtered copper, giving a uniform distribution of nanoparticles in transmission electron microscopy. To demonstrate the application potential, W nanoparticles stabilized nanograined Cu at 500 °C; pure Cu reference showed significant grain growth. This method opens new possibilities in tailored nanocomposite fabrication.

© 2020 Acta Materialia Inc. Published by Elsevier Ltd.  
This is an open access article under the CC BY-NC-ND license.  
(<http://creativecommons.org/licenses/by-nc-nd/4.0/>)

The properties of a material can be improved by altering the structure at the nanoscale in many different ways. For example, the microstructure can be modified either during or after fabrication by means of grain refinement or the incorporation of nanotwins, which will generally increase the strength of the material [1,2]. A nanoscale architecture can be introduced into the sample structure to modify the density, surface area, and mechanical behavior of a material [3–5]. One or more additional phases can also be formed in the structure, often with the goal of increasing the strength or thermal stability of the material [6,7].

Nanoparticles are commonly incorporated into bulk materials as an alternate phase. When nanoparticles are freestanding, their nanoscale dimensions, surfaces, and coatings can be tuned to produce vivid colors, strong sensing capabilities, magnetic effects, and other attractive material properties [8–15]. Their nanoscale features cause them to exhibit physical and chemical properties which are very different from their bulk counterparts, spurring much research into their fabrication and utilization. When nanoparticles are incorporated into a matrix, they can enhance the strength, thermal stability, and optical properties of the composite material; thus, a variety of methods have been developed for incorporating nanoparticles into a matrix material [16–19]. One common method is supersaturation of a material with another element and subsequent

heat treatments to promote the formation of precipitates, often used in nickel superalloys and age-hardened aluminum alloys. Such an approach requires that the materials have significant miscibility at reasonably low temperatures and that the precipitates form with the desired shapes and size distributions.

To avoid the requirement of miscibility, the materials can also be deposited in a non-equilibrium state (e.g. by physical vapor deposition or ion implantation) prior to annealing [20–23]. However, precipitate shapes and spatial distributions are not easily controlled by annealing [24]. Other methods consist of incorporating existing nanoparticles or agglomerated metal ions into a matrix, using methods such as sol-gel suspension, CVD, etc [25–33]. However, such methods are limited in nanoparticle/matrix material selection, due to diffusion caused by the elevated temperatures of deposition, chemical reactivity considerations, and the limited availability of deposition routes for certain materials [12,25,32,34]. In addition, it is often difficult to control the nanoparticle sizes independently of other deposition parameters and avoid agglomeration of the nanoparticles.

In the present study, a novel method for incorporating nanoparticles in a controlled manner into an arbitrary matrix material is demonstrated. Here, the Cu matrix was deposited by magnetron sputtering, while W nanoparticles were synthesized using terminated gas condensation and subsequently ejected onto the substrate during the concurrent Cu deposition. Terminated gas condensation has previously been used to produce single element (and occasionally two element) metal and semiconductor nanoparticles

\* Corresponding author.

E-mail address: [thomas.edwards@empa.ch](mailto:thomas.edwards@empa.ch) (T.E.J. Edwards).

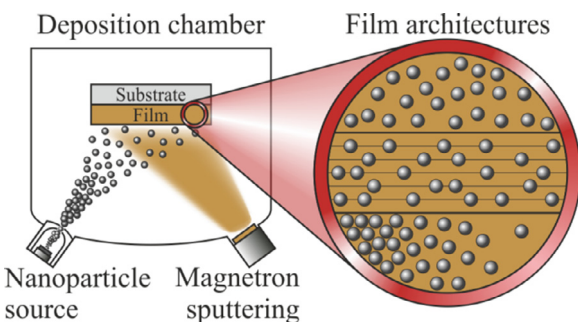


**Fig. 1.** Co-deposition schematic. The nanoparticle source and sputtering source deposit simultaneously onto the substrate, allowing for tailored film architectures.

by DC or radio frequency plasma sputtering followed by extraction of grown clusters through a differential pumping chamber; source parameter optimization has recently been extensively studied [35–39]. The W nanoparticles here were uniformly distributed into the Cu matrix and the sample demonstrated significantly improved resistance to grain growth compared to a pure Cu film deposited under identical conditions. With this deposition method, the matrix and nanoparticle material selection is free from many of the phase diagram and thermodynamic considerations that can dominate for precipitation-formed particles. In addition, the size of the nanoparticles can be controlled by mass selection using a setup akin to a mass spectrometer, which is critical for optical applications [9,11,17,27,40]. Thus, this study demonstrates a new level of control that is now available for the fabrication of nanocomposites and control of their properties.

The samples were deposited using a custom QPREP 500 PVD chamber from Mantis Deposition Ltd, allowing co-deposition of nanoparticles during physical vapor deposition; a schematic of the deposition chamber is shown in Fig. 1. Two types of films were deposited: pure Cu reference films and a second with incorporated W nanoparticles. Sample films were deposited onto carbon film Transmission Electron Microscopy (TEM) grids and Si (100) wafers. Copper was magnetron sputtered from a 76 mm high purity target using a HiPIMS power source (HiPSTER 1, Ionautics AB); tuning the pulse properties allows for unique grain-size control and obtaining a non-porous copper layer. The developed process parameter set keeps twin formation to a minimum. In addition, the highly energized sputtered copper adatoms have a higher mobility upon landing onto the substrate and enhance the embedding of the tungsten particles into the matrix. The average driving current was set to 25 mA and the plasma power to 20 W. The pulse length was 40 µs, with a 300 Hz repetition rate. This reached a peak current of 2 A and a pulse charge of 140 µC. An 8 standard cubic centimeter per minute (scm) argon flow was regulated to produce a 1.7e-3 mbar process pressure using a throttle valve.

W nanoparticles were produced by a 51 mm magnetron head driven by a DC power source. The nanoparticles are formed in an aggregation zone and then a pressure difference extracts the nanoparticles through the exit aperture [41]. To successfully incorporate the tungsten nanoparticles into the matrix, the pressure set-points of various regions of the vacuum system were optimized. These included the nanoparticle aggregation zone, the substrate zone, the magnetron sputtering of the matrix material, and the trajectory of the particles starting from the aggregator exit aperture. The aperture width was matched so that the pressure difference at the exit of the aggregation zone enabled both the extraction of the particles towards the substrate and maintained the terminated gas condensation mechanism, resulting in the desired particle diameters. The current was set to 250 mA, resulting in an average plasma power of 75 W. The magnetron was inserted 80 mm deep

into the nanoparticle aggregation zone and maintained at 20 °C by external cooling. An argon flow of 65 sccm builds 2e-1 mbar pressure within the aggregation zone. The exiting argon flow creates 1e-3 mbar pressure at the aperture, and a residual 5e-4 mbar pressure within the main chamber. This background pressure due to the nanoparticle source operation is compensated by regulating the main chamber pressure with a throttle valve and does not significantly influence the magnetron sputtering of the matrix material.

During deposition, the extracted nanoparticle beam was also driven through a quadrupole mass spectrometer (NanoGen 50, Mantis Deposition Ltd.) to measure the mass distribution of the nanoparticle beam, which is then converted to a nanoparticle diameter distribution. The mass spectrometer also provides the option of nanoparticles size-filtering, which is a limitation for many other techniques, wherein the nanoparticle size is generally coupled with another parameter such as volume fraction [31]. Some possible film architectures which can be fabricated with such a system are diagrammatized in Fig. 1 and illustrated in the supplementary material Figure S1.

The nanocomposite films deposited onto carbon film grids were cleaned in an oxygen plasma cleaner (PlasmaPrep2, GaLa instrumente) and subsequently annealed in vacuum (starting vacuum: <2.5e-5 mbar), first to 300 °C for 3 h and then to 500 °C for 2 h, using a Carbolite STF 16/450 tube furnace. The films deposited onto carbon film grids were directly imaged in plan-view by TEM (JEM2200fs, JEOL) at 200 kV; additionally, TEM cross-sections of an as-deposited Cu film with W nanoparticles on a Si substrate and an annealed Cu film with W nanoparticles on a carbon film TEM grid were prepared using a Tescan-Vela focused ion beam microscope and subsequently imaged by TEM. The cross-sectional TEM sample of the annealed film was taken from the carbon film TEM grid sample rather than the film on the Si substrate, because silicides formed upon annealing of Cu on Si. Chemical analysis was performed by STEM-EDX (Titan Themis, FEI) at 300 kV using a SuperEDX detector system.

Bright-field scanning TEM (BF-STEM) and Dark-field STEM (DF-STEM) images of the as-deposited samples with and without W nanoparticles are shown in Fig. 2. Fig. 2a–c show the sample with W nanoparticles, with the nanoparticles generally appearing darker than the Cu in BF-STEM images and brighter in DF-STEM images through atomic contrast. Further EDX-based chemical analysis is reported in the supplementary material Figure S2. The nanoparticle density by volume,  $n$ , was determined by counting more than 600 nanoparticles in DF-STEM images; particle spacing measurement assumed an ideal gas law distribution, where the center-to-center spacing is approximated by  $0.893(\frac{3}{4\pi n})^{1/3}$ . The average nanoparticle spacing was determined to be 9.5 nm and the nanoparticles were measured to have an average diameter of 4.0 nm, with a standard deviation of 0.7 nm. This particle size matches that measured by the mass spectrometer during deposition, where a 4.0 nm average diameter was measured, with a standard deviation of 1.3 nm.

The samples did not show agglomeration of nanoparticles. In addition, in Fig. 2c, the nanoparticles are scattered throughout the Cu grains, not just at grain boundaries. Therefore, the nanoparticles do not cause renucleation events; rather, the Cu grains appear to be simply growing around the W nanoparticles. This is in contrast to the renucleation due to nanoparticles that is sometimes observed for other deposition methods, such as Pt and Au nanoparticles in CVD ZnO [42].

A plan view of as-deposited pure Cu is shown in Fig. 2d. The grain shapes are qualitatively similar for the samples with and without W nanoparticles, and the average Cu grain diameters are  $28 \pm 11$  nm for the sample with W nanoparticles and  $25 \pm 11$  nm for the sample without W nanoparticles. Grain sizes were deter-

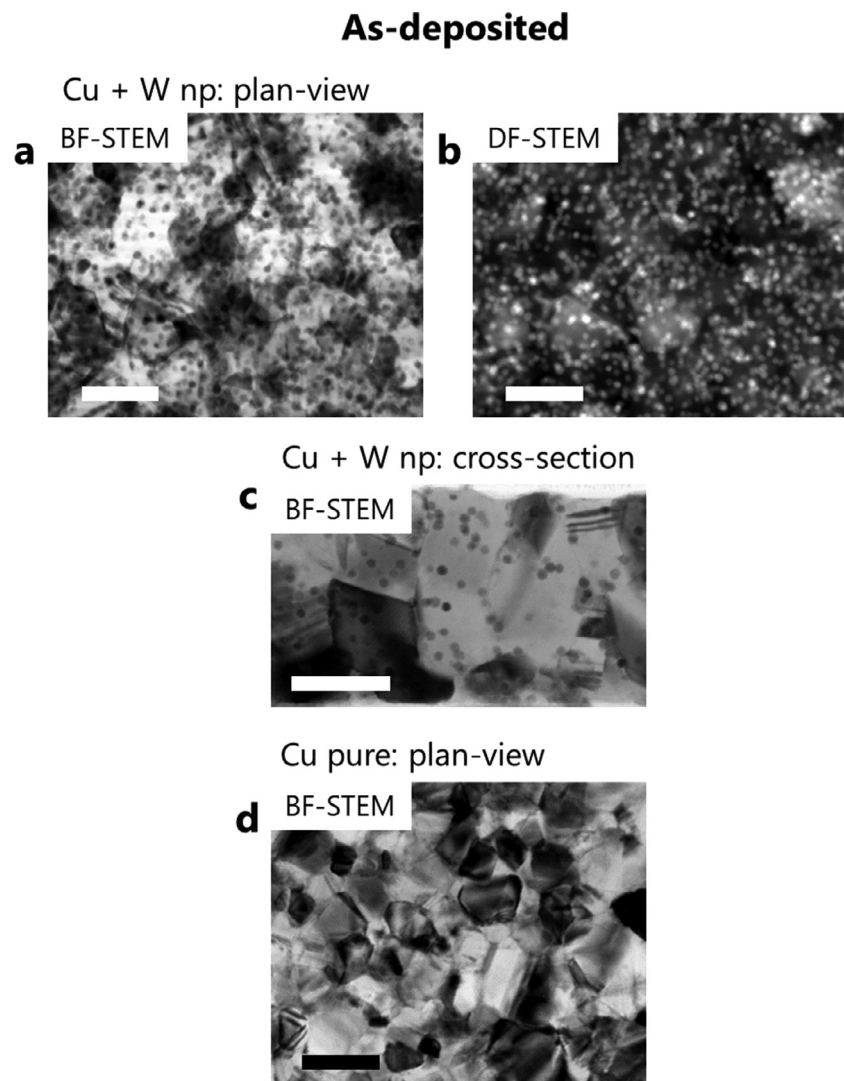


**Fig. 2.** TEM images of as-deposited Cu films with and without W nanoparticles (np). a) BF-STEM plan-view image showing the grain structure of the Cu and the distribution of W nanoparticles (dark dots). b) DF-STEM image of the same area as a); here W nanoparticles appear as bright dots. c) Cross-sectional BF-STEM image of a Cu film with W nanoparticles. d) BF-STEM plan-view image of a pure Cu film. For both compositions, the average Cu grain size is similar at 28 and 25 nm, with and without W, respectively. All scale bars are 50 nm.

mined from TEM images and are “column diameter” values, since the Cu grains are columnar rather than spherical. Overall, the two samples start with similar microstructures and grain sizes.

TEM images of the films after annealing to 500 °C in vacuum for 2 h are shown in Fig. 3. The grain structure of the annealed sample with W nanoparticles remains similar to that before annealing. The Cu grain diameter increased slightly from 28 nm to  $36 \pm 13$  nm after annealing, and the W nanoparticles are still dispersed: many particles remain at the grain interiors rather than the grain boundaries. This retention of nanoparticle dispersion is similarly seen in the cross-section images, Fig. 3d.

In contrast, there was significant grain growth for the sample without W nanoparticles, as in Fig. 3e. The average grain diameter increased from 25 nm to  $118 \pm 54$  nm after annealing. This stark difference in grain growth is evident in the DF-TEM images in Fig. 3c and f (with and without W nanoparticles), noting the scale-bar change. In Fig. 3e, twin boundaries are evident; these are also present in the as-sputtered Cu grains for both samples, but are less evident as the as-sputtered grains are smaller.

The overall W composition of the sample, based on an average particle diameter of 4 nm spaced at 9.5 nm, is ~ 0.75 vol.%.

Thus, this small volume of nanoparticles was sufficient to significantly inhibit the grain growth of the nanocrystalline Cu, even at 0.57 homologous temperature for 2 h. In fact, one may consider the pinning potential of the W nanoparticles with radius  $r$  on the growth of Cu grains, radius  $R_c$ , according to the generalized Zener drag equation<sup>43</sup>:

$$R_c = \frac{Kr}{f^m}$$

where the prefactor  $K$ , and the exponent  $m$  of the particle volume fraction,  $f$ , have been determined experimentally for a range of insoluble and precipitate particles in engineering alloys to be best valued at 0.17 and 1, respectively, for  $f < 0.05$ , as here. For 4 nm diameter W particles at 0.7 vol.% this yields Cu grains of 91 nm diameter – somewhat larger than the measured values following heat treatment, but nevertheless lower than the Cu grain size in the absence of W nanoparticles. In fact, further investigations into Zener drag [38] have shown that, as here, additional grain refinement occurs when the particles are stable, and the initial grain size is both refined and homogeneous.

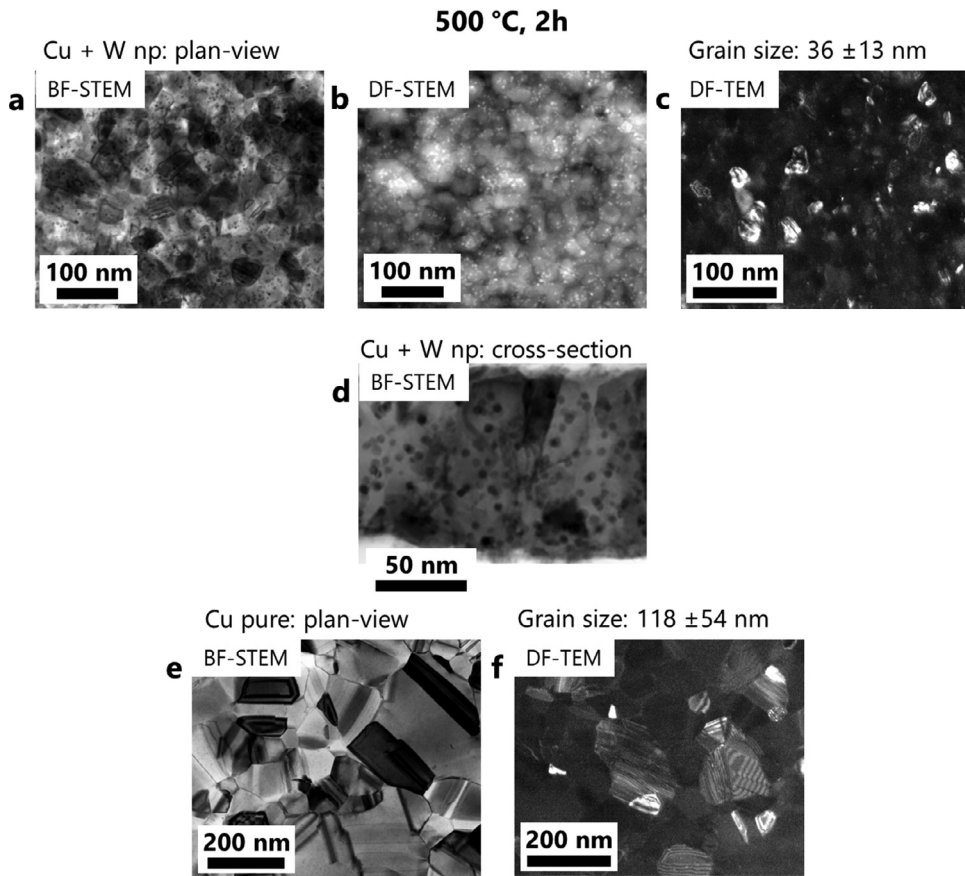


**Fig. 3.** TEM images of annealed ( $500\text{ }^{\circ}\text{C}$ , 2 h) Cu films with W nanoparticles (plan view - a, b, c; cross-sectional view - d) and without W nanoparticles (plan view - e, f). Note the change in scale-bar in e and f: the grain growth is considerable for the pure Cu sample.

The stability of the nanoparticles results from two important considerations: W is immiscible in Cu, and W has a high melting point (3695 K vs. 1358 K for Cu). These two properties are of note for demonstrating the flexibility of this method of co-deposition. To alternatively have W distributed in Cu would require co-sputtering of both materials (since they are immiscible), as has been previously performed for a variety of compositions [23]. However, subsequent annealing of such co-sputtered material may not result in the desired structure, since annealing affects both phases and independent control of the two structural components (matrix and nanoparticles) is hence lost, i.e. Cu grains can grow before the W nanoparticles are completely formed by segregation. On the other hand, direct deposition of the W nanoparticles into the Cu as performed here allows for a controlled and thermally-stable as-deposited structure.

The small amount of W that was required to effect this increased thermal stability also holds promise for producing materials with certain significantly improved properties (thermal stability, optical properties, strength), while causing minimal alterations to other properties (electrical and thermal conductivity, density, corrosion resistance), as the majority phase remains unalloyed. Further control of the nanoparticle distribution can also be implemented by having nanoparticles embedded both randomly and in layers, with lateral and depth gradients in particle density also possible. This allows for additional tuning of the material properties, see diagram, Fig. 1, and micrographs, Figure S1.

The flexibility of the deposition method also lends itself favorably to the possibility of creating model systems to verify fundamental theories in Materials Science, such as Zener drag evoked here, but also particle strengthening in materials mechanics, and

the kinetics of elemental interdiffusion. Indeed, an idealized starting state for diffusion studies can be generated with this method: a mechanical mixture with a uniform 3D distribution of point sources of pure elements in a pure matrix. Similarly in the case of the Zener theory [43], the core assumptions are fulfilled by the present co-deposited system: the W particles are reasonably approximated as spherical, although the Cu grains are themselves columnar, which facilitates use of a 2D model, the particles are incoherent in the matrix and are uniformly distributed, and finally the particle sizes are narrowly distributed and are small enough relative to the initial grain size to interact with only one grain boundary at a time.

Therefore, a method for co-deposition of nanoparticles into a matrix has been demonstrated that has the same material-selection versatility, which is provided by conventional magnetron sputtering. This technique avoids the thermodynamic considerations, which are inherent to most other nanocomposite co-deposition methods, resulting in many new possible matrix-nanoparticle material combinations. The nanoparticles can be randomly distributed throughout the material, as was done here, or the spatial distribution can be controlled by varying the deposition parameters and interrupting the nanoparticle or matrix deposition as needed. As was demonstrated for Cu in this study, thermal stability could be immediately improved using such a deposition method. This technique also holds promise for producing materials with tuned optical properties, where nanoparticle sizes and distributions need to be well controlled. Finally, this technique allows for the fabrication of tailored microstructures for fundamental investigations of nanocomposite behavior during mechanical deformation and in other conditions. Overall, this deposition method

lends significant flexibility and control to the field of nanocomposite fabrication.

### Declaration of Competing Interests

The authors declare that they have no known competing financial interests or personal relationships that could have appeared to influence the work reported in this paper.

### Acknowledgements

T.E.J.E. acknowledges the EMPAPOSTDOCS-II program which has received funding from the European Union's Horizon 2020 research and innovation program under the Marie Skłodowska-Curie grant



agreement number 754364.

### Supplementary materials

Supplementary material associated with this article can be found, in the online version, at doi:10.1016/j.scriptamat.2020.05.032.

### References

- [1] L. Lu, Y. Shen, X. Chen, L. Qian, K. Lu, *Science* 304 (2004) 422–426.
- [2] S. Zheng, I.J. Beyerlein, J.S. Carpenter, K. Kang, J. Wang, W. Han, N.A. Mara, *Nat. Commun.* 4 (2013) 1696–1698.
- [3] T.A. Schaedler, A.J. Jacobsen, A. Torrents, A.E. Sorensen, J. Lian, J.R. Greer, L. Valdevit, W.B. Carter, Q. Ge, J.A. Jackson, S.O. Kucheyev, N.X. Fang, C.M. Spadaccini, *Science* 334 (2011) 962–965.
- [4] L.R. Meza, S. Das, J.R. Greer, *Science* 345 (2014) 1322–1326.
- [5] J. Erlebacher, M.J. Aziz, A. Karma, N. Dimitrov, K. Sieradzki, *Nature* 410 (2001) 450–453.
- [6] T. Chookajorn, H.a Murdoch, C.a Schuh, C.A.S. Tongjai Chookajorn, Heather A. Murdoch, *Science* (80-.), 337 (2012) 951–954.
- [7] T.J. Rupert, *Curr. Opin. Solid State Mater. Sci.* 20 (2016) 257–267.
- [8] G. Walters, I.P. Parkin, *J. Mater. Chem.* 19 (2009) 574–590.
- [9] H.A. Atwater, A. Polman, *Nat. Mater.* 9 (2010) 205–213.
- [10] M. Kerker, *Scatt. Light Other Electromagn. Radiat.* 16 (1969) 27–96.
- [11] J.A. Scholl, A.L. Koh, J.A. Dionne, *Nature* 483 (2012) 421–427.
- [12] J.N. Anker, W.P. Hall, O. Lyandres, N.C. Shah, J. Zhao, R.P. Van Duyne, *Nat. Mater.* 7 (2008) 442–453.
- [13] Y. Qiang, Y. Qiang, R.F. Sabiryanov, R.F. Sabiryanov, S.S. Jaswal, S.S. Jaswal, Y. Liu, Y. Liu, H. Haberland, D.J. Sellmyer, D.J. Sellmyer, *Phys. Rev. B - Condens. Matter Mater. Phys.* 66 (2002) 644041–644044.
- [14] S.H. Baker, M. Roy, S.C. Thornton, C. Binns, *J. Phys. Condens. Matter* 24 (2012) 176001.
- [15] D.A. Eastham, Y. Qiang, T.H. Maddock, J. Kraft, J.P. Schille, G.S. Thompson and H. Haberland, *J. Phys. Condens. Matter*, doi:10.1088/0953-8984/9/37/001.
- [16] I.A. Ibrahim, F.A. Mohamed, E.J. Lavernia, *J. Mater. Sci.* 26 (1991) 1137–1156.
- [17] K. Awazu, M. Fujimaki, C. Rockstuhl, J. Tominaga, H. Murakami, Y. Ohki, N. Yoshida, T. Watanabe, *J. Am. Chem. Soc.* 130 (2008) 1676–1680.
- [18] R.G. Palgrave, I.P. Parkin, *Chem. Mater.* 19 (2007) 4639–4647.
- [19] M.K. Kwon, J.Y. Kim, B.H. Kim, I.K. Park, C.Y. Cho, C.C. Byeon, S.J. Park, *Adv. Mater.* 20 (2008) 1253–1257.
- [20] H.B. Liao, R.F. Xiao, J.S. Fu, P. Yu, G.K.L. Wong, P. Sheng, *Appl. Phys. Lett.* 70 (1997) 1–3.
- [21] R.H. Magruder III, L. Yang, R.F. Haglund, C.W. White, R. Dorsinville, R.R. Alfano, *Appl. Phys. Lett.* 62 (1993) 1730–1732.
- [22] K. Fukumi, A. Chayahara, K. Kadono, T. Sakaguchi, Y. Horino, M. Miya, J. Hayakawa, M. Satou, *Jpn. J. Appl. Phys.* 30 (1991) L742–L744.
- [23] F.T.N. Vüllers, R. Spolenak, *Acta Mater.* 99 (2015) 213–227.
- [24] S. Johnsen, J. He, J. Androulakis, V.P. Dravid, I. Todorov, D.Y. Chung, M.G. Kanatzidis, *J. Am. Chem. Soc.* 133 (2011) 3460–3470.
- [25] R. Serna, C.N. Afonso, C. Ricolleau, Y. Wang, Y. Zheng, M. Gandais, I. Vickridge, *Appl. Phys. A* 71 (2000) 583–586.
- [26] W. Wang, L. Qu, G. Yang, Z. Chen, *Appl. Surf. Sci.* 218 (2003) 24–28.
- [27] R. Serna, A. Suárez-García, C.N. Afonso, D. Babonneau, *Nanotechnology* 17 (2006) 4588–4593.
- [28] Z. Konstantinović, M.G. Del Muro, M. Varela, X. Batlle, A. Labarta, *Nanotechnology* 17 (2006) 4106–4111.
- [29] N. Bahlawane, K. Kohse-Höinghaus, T. Weimann, P. Hinze, S. Röhe, M. Bäumer, *Angew. Chemie - Int. Ed.* 50 (2011) 9957–9960.
- [30] S.K. Medda, S. De, G. De, *J. Mater. Chem.* 15 (2005) 3278.
- [31] S.F. Hassan, M. Gupta, *Metall. Mater. Trans. A* 36 (2005) 2253–2258.
- [32] U. Kreibig, C. v. Fragstein, *Z. Phys* 224 (1969) 307–323.
- [33] R.G. Palgrave, I.P. Parkin, *J. Am. Chem. Soc.* 128 (2006) 1587–1597.
- [34] D. Bekermann, D. Barreca, A. Gasparotto, C. Maccato, *CrystEngComm* 14 (2012) 6347.
- [35] T. Hihara, K. Sumiyama, *J. Appl. Phys.* 84 (1998) 5270–5276.
- [36] S. Yamamoto, K. Sumiyama, K. Suzuki, *J. Appl. Phys.* 85 (1999) 483–489.
- [37] S. Sawa, N. Tanaka, R. Katoh, K. Sumiyama, *Mater. Trans.* 49 (2008) 1219–1222.
- [38] K. Sumiyama, T. Hihara, D.L. Peng, R. Katoh, *Sci. Tech. Adv. Mater.* 6 (2005) 18–26.
- [39] M. Khojasteh, V.V. Kresin, *Appl. Nanosci.* 7 (2017) 875–883.
- [40] Y. Wang, J. Hu, Y. Lin, C.W. Nan, *NPG Asia Mater* 2 (2010) 61–68.
- [41] A.H. Kean, L. Allers, *NSTI Nanotechnol. Conf. Trade Show - NSTI Nanotech 2006 Tech. Proc.* 1 (2006) 749–752.
- [42] A. Salaün, J.A. Hamilton, D. Iacopino, S.B. Newcomb, M.G. Nolan, S.C. Padmanabhan, I.M. Povey, M. Salaün, *Thin Solid Films* 518 (2010) 6921–6926.
- [43] P.A. Manoharm, M. Ferry, T. Chandra, *ISIJ Int.* 38 (1998) 913–924.